Supporting Information

Denghui Wang,‡ [a,c] Minghao Ma,‡ [a,b] Wenqiang Xu, [a,b] Yingjie Ma,*[a] Lidong Li,*[b] and Xianglong Li*[a,c]

[a] CAS Key Laboratory of Nanosystem and Hierarchical Fabrication, CAS Center for Excellence in Nanoscience, National Center for Nanoscience and Technology, Beijing, 100190, China.

[b] State Key Laboratory for Advanced Metals and Materials, School of Materials Science and Engineering, University of Science and Technology Beijing, Beijing, 100083, China.

[c] University of Chinese Academy of Sciences, Beijing, 100049, China.

*Corresponding author, email addresses: lixl@nanoctr.cn; lidong@mater.ustb.edu.cn; mayj@nanoctr.cn

‡ These authors contributed equally.

Experimental Section

Fabrication of LS: 2 g of commercial $Li_{13}Si_4$ (China Energy Lithium Co., Ltd.) was carefully added to 500 mL of ethyl alcohol (analytically pure, Macklin) in an ice bath under a nitrogen atmosphere, stirred for two h, and filtered. The obtained sediment was washed with acetic acid (analytically pure, Macklin) and deionized water, dried in a vacuum oven at 80 °C, and then further heated at 650 °C for one hour in an Ar atmosphere, giving LS.

Fabrication of 3DS: the as-prepared LS was mixed with metallic lithium flakes (China Energy Lithium Co., Ltd.) in a weight ratio of 1.5:1 in a nickel crucible and heated at 350 °C for one hour under an Ar atmosphere, producing Li_xSi. These operations were carried out in a glove box filled with an inert atmosphere (water and oxygen concentrations less than 0.1 ppm) to prevent lithium flakes and silicide alloy powder oxidation. The prepared LixSi powder was delithiated in a manner analogous to the preparation of LS, yielding 3DS.

Fabrication of 3DS@C: 600 mg of 3DS was dispersed in 150 ml of Tris-HCl buffer solution (pH approximately 8.4), and 200 mg of dopamine hydrochloride was added, then sonicated and stirred for two hours. In the final step, the precipitate was collected by vacuum filtration and dried under vacuum at 80 °C for 12 h, then further heated at 850 °C under an Ar/H_2 (9:1) atmosphere for two hours with a heating rate of 5 °C min^{-1}, thus yielding 3DS@C.

Material Characterization: SEM (FE-SEM, Hitachi SU8220) and TEM (FE-TEM, FEI Tecnai G2 20 STWIN, and Tecnai G2 F20 U-TWIN) tests were used to reveal the microstructure of the as-obtained products. The XRD were measured between 5° and 80° by D/MAX-TTRIII X-ray diffractometer (Cu kα radiation, $\lambda = 0.15418$ nm). TGA tests were performed in airflow from room temperature to 900 °C at a heating rate of 5 °C min^{-1}. Nitrogen adsorption/desorption isotherms were obtained at 77 K with an ASAP 2020 physisorption analyzer. The Brunauer-Emmett-Teller (BET) method and Barrett-Joyner-Halenda (BJH) model were used to estimate the specific surface area and the pore width distribution, respectively. Raman spectra were collected using a Renishaw in Via Raman microscope with a laser wavelength of 514.5 nm. ESCALAB250Xi apparatus with an Al Kα X-ray source was used to perform X-ray Photoelectron Spectroscopy (XPS) measurements. The powder's electrical resistivities were measured by a ST2742C Automatic Powder Resistivity Tester (Suzhou Jingge Electronic Co., Ltd.).

Electrochemical Characterization: CR2032 coin-type cells were used to perform the electrochemical measurements. The working electrode was made by spreading a slurry

of 70 wt.% active materials (LS, 3DS, and 3DS@C), 20 wt.% conductive additive (Super P, Alfa Aesar), and 10 wt.% polyacrylic acid (PAA, weight-average molecular weight of 240 000, Alfa Aesar), then dried at 60 °C for the last 12 hours. Half-cells were assembled in an Ar-filled glove box (<0.1 ppm of oxygen and water), with lithium metal as the counter electrode.

Cycling and rate capability tests were performed using a CT2001A battery program controlling test system, operating in the voltage range of 0.01 to 1.0 V. All electrochemical measurements, unless otherwise stated, were conducted at ambient temperature. The capacity reported was determined based on the total weight of active materials in the working electrode and the cycling conditions as annotated.

Areal capacity was calculated by multiplying the gravimetric capacity with the areal mass loading of active materials. Similarly, Coulombic efficiency was determined by dividing delithiation capacity by lithiation capacity. Electrochemical impedance spectroscopy (EIS) assessments were performed with frequencies ranging from 0.01 Hz to 100 kHz using a Biologic electrochemical workstation.

Reaction kinetics were observed by employing the Galvanostatic Intermittent Titration Technique (GITT), where a pulse current of 100 mA g^{-1} was applied for 20 minutes between 20-minute rest intervals. Fick's second law was used along with a simplified equation to determine the apparent diffusion coefficient of Li.

$$D = \frac{4}{\pi\tau}\left(\frac{m_B V_M}{M_B S}\right)^2\left(\frac{\Delta E_S}{\Delta E_\tau}\right)^2$$

Where mB and M_B are the active mass and molecular mass, respectively, V_M is the molar volume, S is the surface area of the electrode, and τ, ΔE_S and ΔEτ are the pulse time for charge and discharge processes, voltage change in the steady state, and voltage change during the pulse period, respectively.

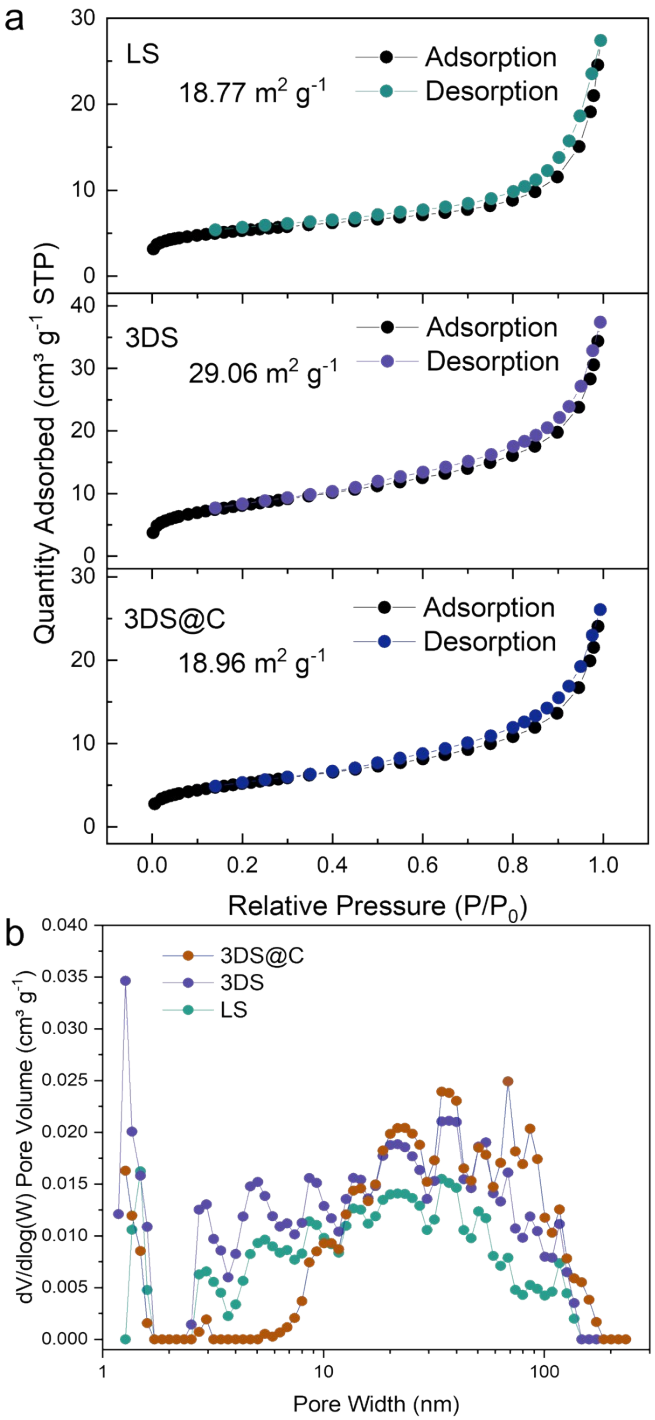

Figure S1. (a) Nitrogen adsorption-desorption isotherms and (b) Pore width distribution distributions of LS, 3DS, and 3DS@C. The Brunauer-Emmett-Teller (BET) method and Barrett-Joyner-Halenda (BJH) model were utilized to estimate the specific surface area and pore width distribution, respectively. The results show the specific surface area of LS, 3DS, and 3DS@C is about 18.77, 29.06, and 18.96 m^2 g^{-1}, respectively.

Table S1. Specific surface area, average pore size and pore volume of LS, 3DS, and 3DS@C

Sample	Specific surface area (m^2/g)	Average Pore size (nm)	Pore volume (cm^3/g)
LS	18.76	8.62	0.405
3DS	29.06	7.98	0.580
3DS@C	18.96	8.96	0.425

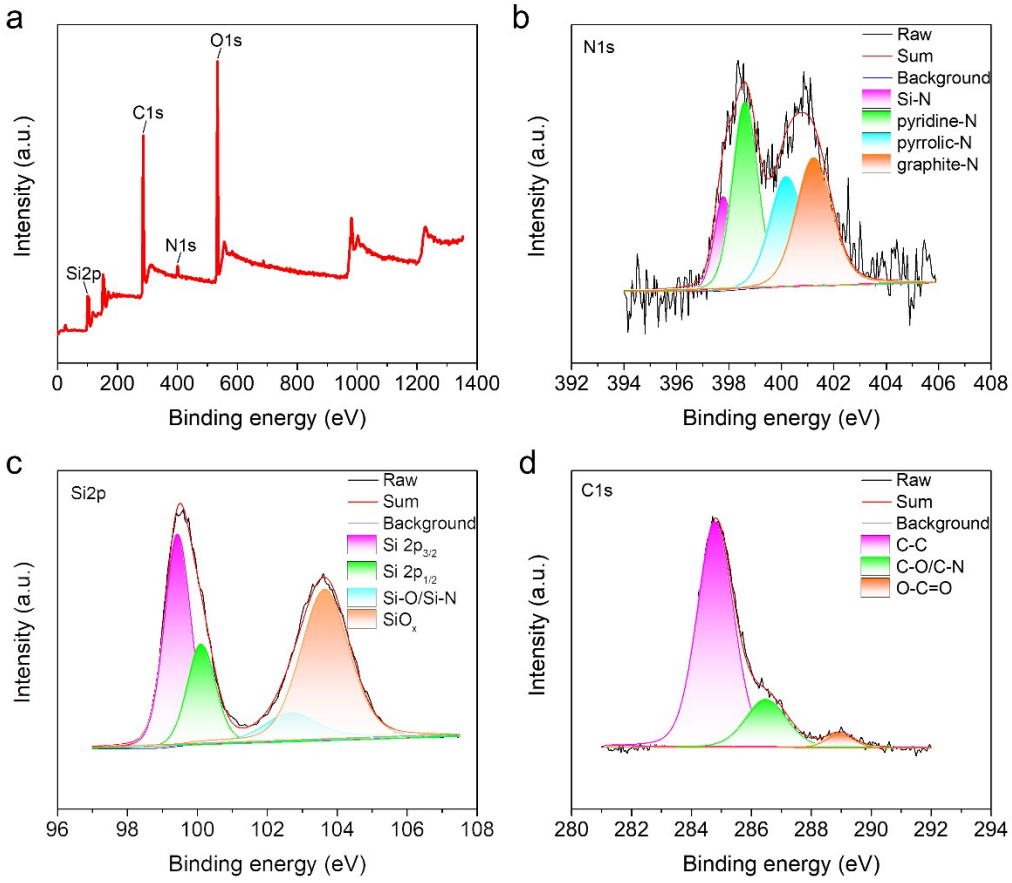

Figure S2. Interfacial and componential characterization of 3DS@C. (a) XPS survey spectra; (b) N1s XPS spectra; (c) Si2p XPS spectra; (d) C1s XPS spectra of 3DS@C.

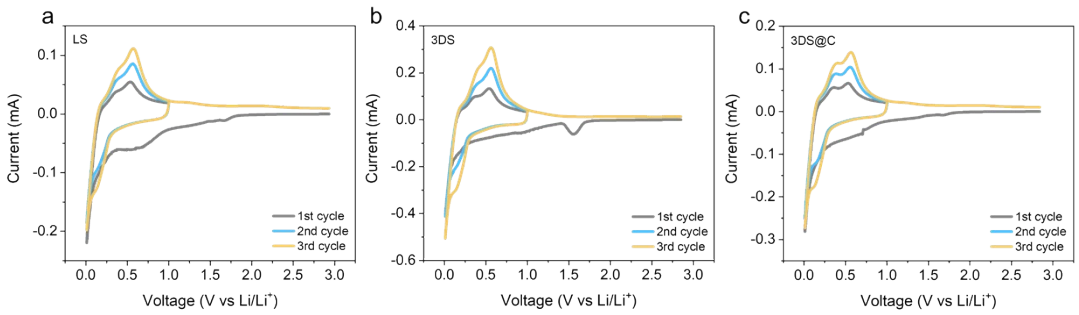

Figure S3. CV curves for the initial three cycles of (a) LS, (b) 3DS, and (c) 3DS@C.

Table S2. Rate capability comparison of 3DS@C and Si/C anode materials in the previous work.

No.	Materials	Voltage window (V)	Capacity (mAh g^{-1})/Current rate (A g^{-1})	Loading (mg cm^{-2})	Ref.
1	3DS@C	0.01~1	2818/0.8; 2529/2; 2281/4; 1733/8; 1346/12; 897.9/16	1.0~1.2	This work
2	Si/LM@C-CNF	0.01~2	1839/1; 1533/5; 1306/1; 1030/2; 702/4; 588/5	1.47	[1]
3	Si-co-HGCS	0.005~1	1974/0.2; 1687/0.5; 1533/1; 1247/2; 932/4; 862/5	1.0~1.5	[2]
4	SHC	0.005~3	1642/0.2; 1399/0.4; 1146/0.8; 918/1.6; 699/3.2	1.0~1.8	[3]
5	VGAs@Si@CNFs-1	0.01~1	3307/0.05; 3206/0.1; 3026/0.2; 2889/0.4; 2767/0.6; 2646/0.8; 2243/1; 2026/2; 1696/4; 1366/6; 1140/8; 1048/10	0.8~1.5	[4]
6	Si/GNs-0.33	0.01~3	1145/0.1; 1087/0.2; 974/0.5; 863/1; 799/2; 667/5	1.35	[5]
7	NPSi@C-700	0.01 ~3	2396/0.1; 2187/0.5; 1954/1; 1760/2; 1561/3; 1447/4; 1278/5	1.5~1.8	[6]
8	Si@C@ZIF-67-800N	0.01~1.5	1488/0.1; 1353/0.5; 1183/1; 980/2; 777/3; 687/5	0.8~1.2	[7]
9	p-Si@C	0.001~2	2081/0.2; 1912/0.4; 1752/0.8; 1704/1; 1479/2; 1172/4	0.6	[8]

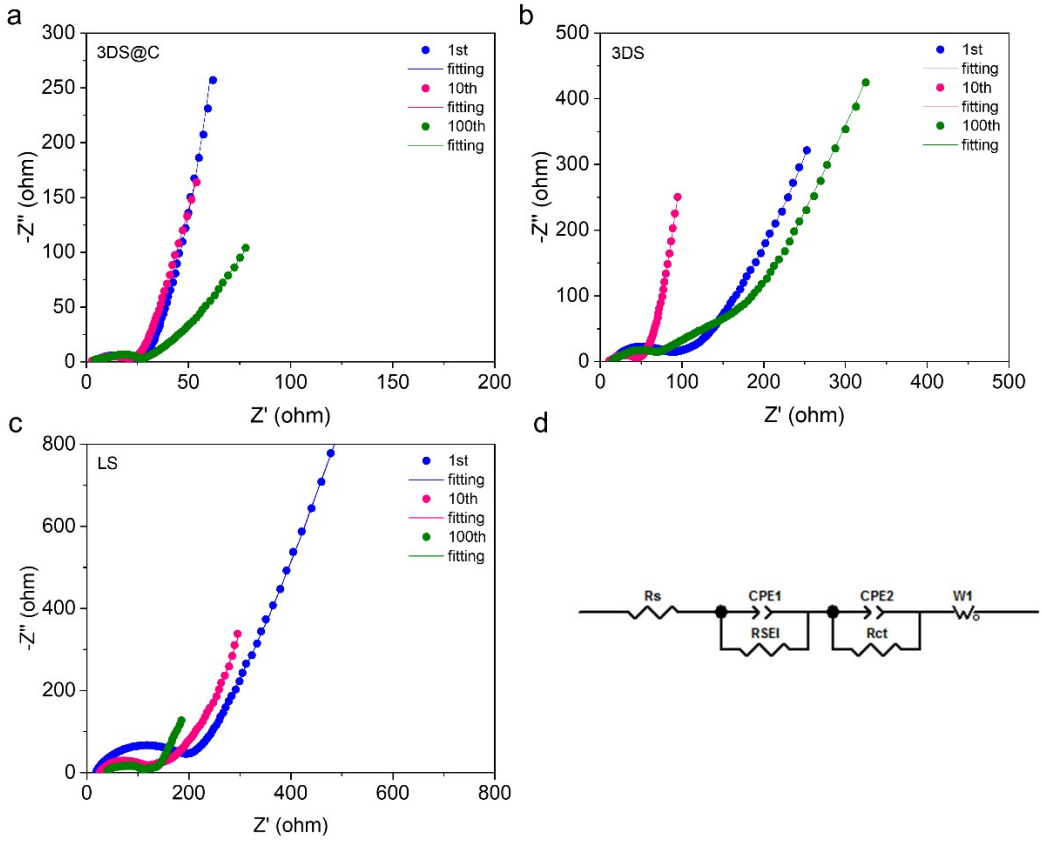

e

	3DS@C			3DS			LS		
	R_s (Ω)	R_{SEI} (Ω)	R_{ct} (Ω)	R_s (Ω)	R_{SEI} (Ω)	R_{ct} (Ω)	R_s (Ω)	R_{SEI} (Ω)	R_{ct} (Ω)
1st	3.2	1.5	20.3	12.3	20.9	55.6	16.8	12.2	131.9
10th	2.3	1.5	14.8	10.2	9.3	29.4	23.7	44.7	111.8
100th	2.6	2.1	15.2	13.1	11.8	54.4	36.1	54.2	86.3

Figure S4. Electrochemical kinetics characterization of (a-c) Nyquist plots of (a) 3DS@C, (b) 3DS, and (c) LS after annotated charge/discharge cycles obtained from EIS measurements. (d) Fitting circuit diagram. (e) The resistance values of 3DS@C, 3DS, and LS.

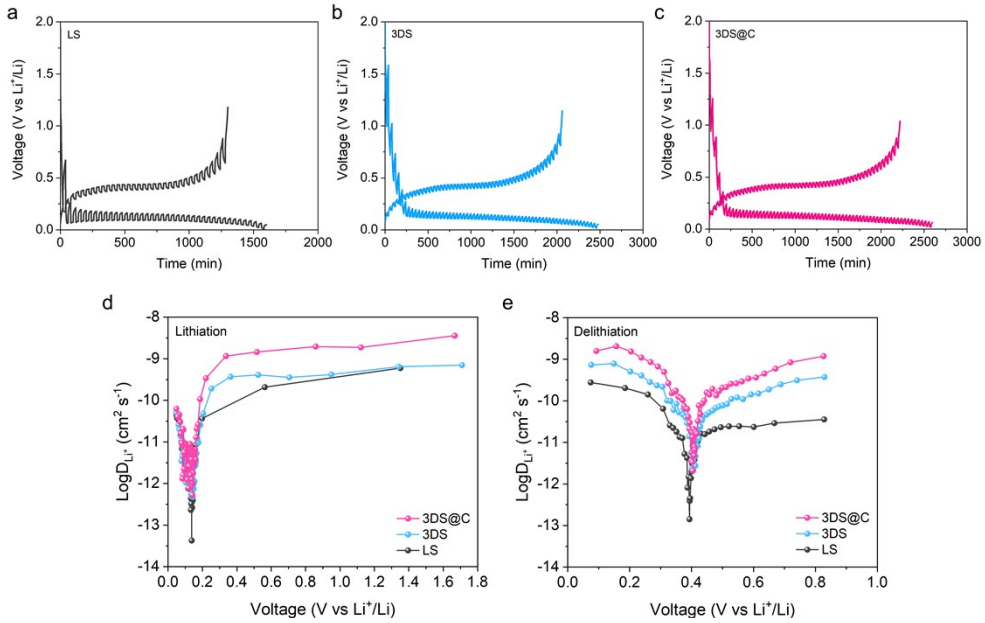

Figure S5. Galvanostatic intermittent titration technique (GITT) measurements of (a) LS, (b) 3DS, and (c) 3DS@C. Li^+ diffusion coefficients of LS, 3DS, and 3DS@C during (d) lithiation and (h) delithiation.

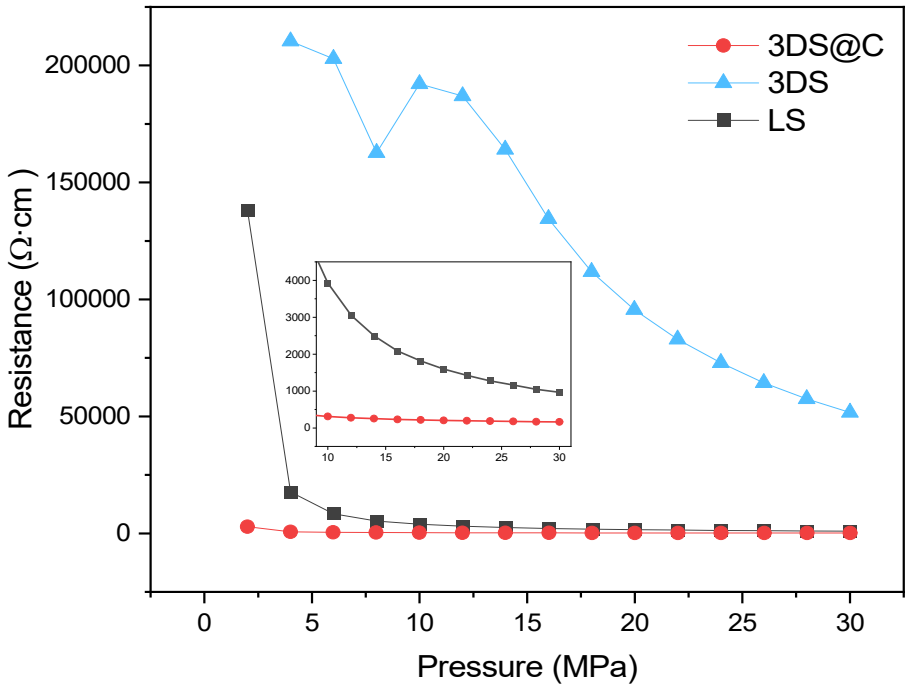

Figure S6. Electrical resistivities of LS, 3DS, and 3DS@C at different pressures.

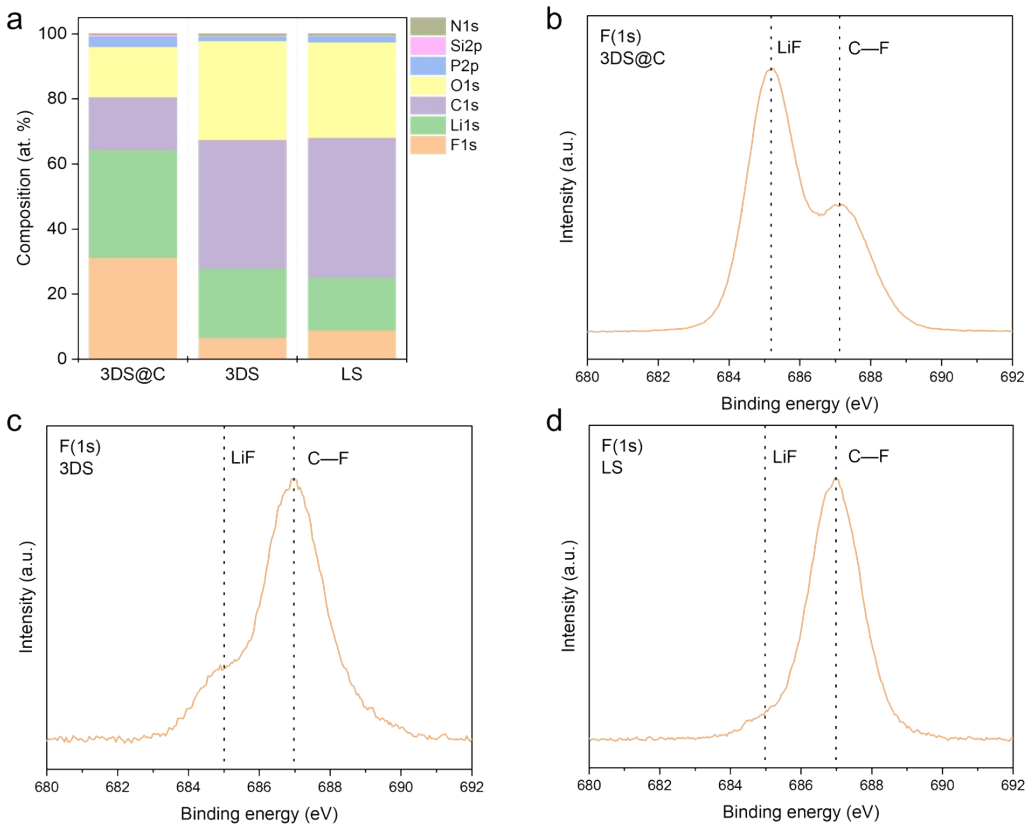

Figure S7. Characterization of SEI: (a) the element composition of 3DS@C, 3DS, and LS anodes after 20 cycles at 2A g^{-1}. F 1s XPS spectra of the SEI of 3DS@C (b), 3DS (c), and LS (d) anodes after 20 cycles at 2A g^{-1}.

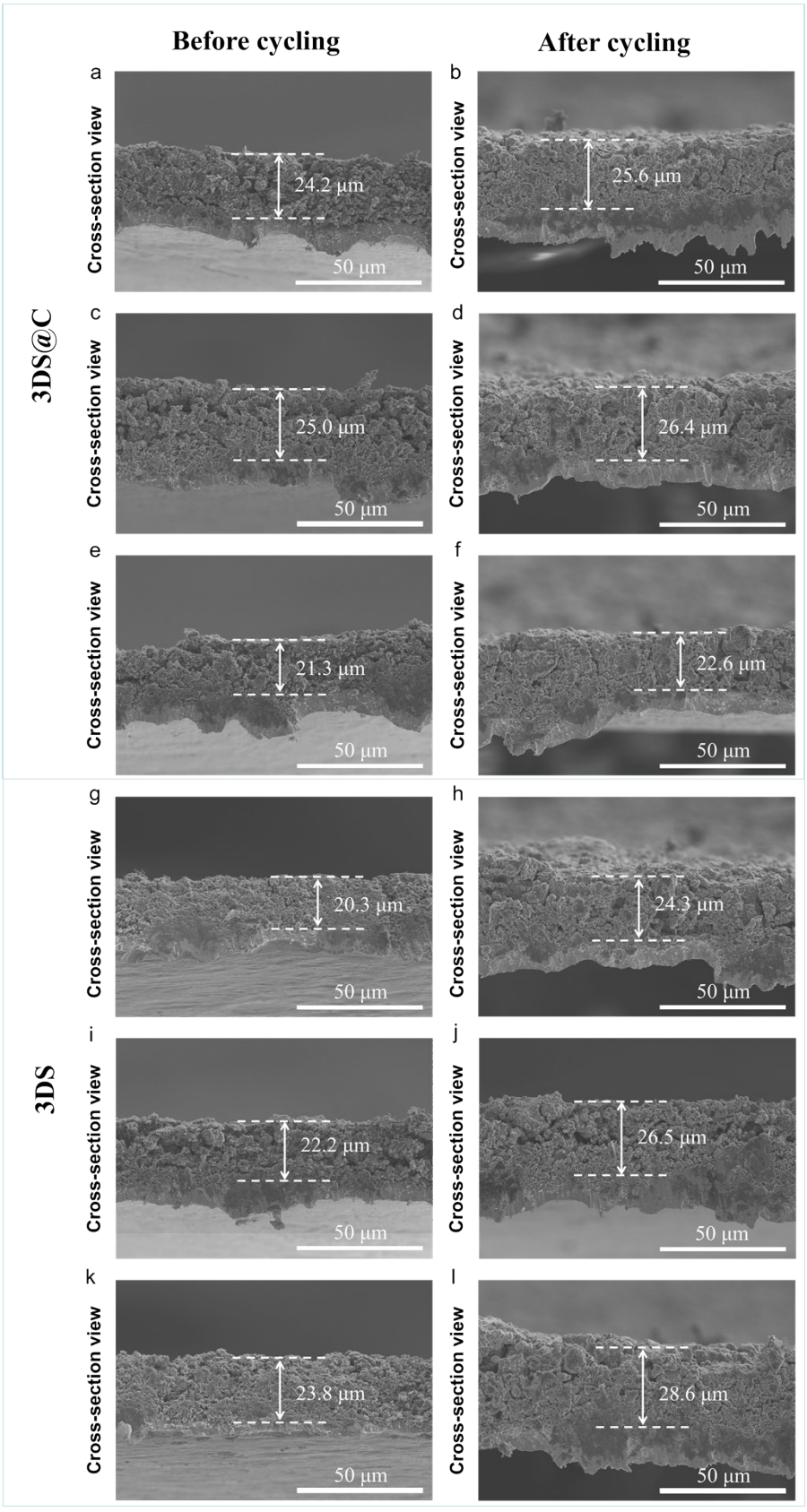

Figure S8. Morphological and structural characterization: SEM images (cross-section view) of the 3DS@C electrodes (a, b, c, d, e, f) and the 3DS electrodes (g, h, i, j, k, l)

before and after cycling 50 cycles at 2A g^{-1}.

We measured the thicknesses of three 3DS@C and three 3DS electrodes before and after cycling and calculated their respective electrode expansion rates. Subsequently, the average value of the three electrode swelling rates was taken as the expansion rates of the 3DS@C (5.8 %) and 3DS (19.7 %) electrodes, respectively.

References

[1] Z. Zhao, J. Han, F. Chen, J. Xiao, Y. Zhao, Y. Zhang, D. Kong, Z. Weng, S. Wu and Q. Yang, Adv. Energy Mater., 2022, 12, 2103565.

[2] Z. Li, Z. Zhao, S. Pan, Y. Wang, S. Chi, X. Yi, J. Han, D. Kong, J. Xiao, W. Wei, S. Wu and Q. Yang, Adv. Energy Mater., 2023, 13, 2300874.

[3] R. Zhu, Z. Wang, X. Hu, X. Liu and H. Wang, Adv. Funct. Mater., 2021, 31, 2101487.

[4] Y. Mu, M. Han, B. Wu, Y. Wang, Z. Li, J. Li, Z. Li, S. Wang, J. Wan and L. Zeng, Adv. Sci., 2022, 9, 2104685.

[5] Y. Zhang, Z. Wang, K. Hu, J. Ren, N. Yu, X. Liu, G. Wu and N. Liu, Energy Storage Mater., 2021, 34, 311–319.

[6] Y. An, Y. Tian, H. Wei, B. Xi, S. Xiong, J. Feng and Y. Qian, Adv. Funct. Mater., 2020, 30, 1908721.

[7] N. Liu, J. Liu, D. Jia, Y. Huang, J. Luo, X. Mamat, Y. Yu, Y. Dong and G. Hu, Energy Storage Mater., 2019, 18, 165–173.34

[8] R. Gao, J. Tang, K. Zhang, K. Ozawa and L.-C. Qin, Nano Energy, 2020, 78, 105341.